PERGAMON

International Journal of Solids and Structures 40 (2003) 3107–3128

INTERNATIONAL JOURNAL OF SOLIDS and STRUCTURES

www.elsevier.com/locate/ijsolstr

Free vibration and spatial stability of non-symmetric thin-walled curved beams with variable curvatures

Nam-Il Kim [a], Kwang-Jin Seo [b], Moon-Young Kim [a,*]

[a] *Department of Civil-Environmental Engineering, SungKyunKwan University, Jangan-Gu, Suwon, Kyoungki-Do 440-746, South Korea*

[b] *Korea Engineering Consultants Corporation, Shinsa-dong, Gangman-gu, Seoul 135-790, South Korea*

Received 22 February 2002; received in revised form 8 February 2003

Abstract

An improved formulation for free vibration and spatial stability of non-symmetric thin-walled curved beams is presented based on the displacement field considering variable curvature effects and the second-order terms of finite-semitangential rotations. By introducing Vlasov's assumptions and integrating over the non-symmetric cross-section, the total potential energy is consistently derived from the principle of virtual work for a continuum. In this formulation, all displacement parameters and the warping function are defined at the centroid axis and also thickness-curvature effects and Wagner effect are accurately taken into account. For F.E. analysis, a thin-walled curved beam element is developed using the third-order Hermitian polynomials. In order to illustrate the accuracy and the practical usefulness of the present method, numerical solutions by this study are presented with the results analyzed by ABAQUS' shell elements. Particularly, the effect of arch rise to span length ratio is investigated on vibrational and buckling behaviour of non-symmetric curved beams.

Keywords: Free vibration; Stability; Thin-walled beam; Variable curvature; FEM

1. Introduction

Curved bridges, arches and thin-walled structural members having variable curvatures show very complex structural behaviour since twisting moments are always occurring in addition to bending moments due to curvature effects. Therefore the accurate prediction of the natural frequencies and the stability limit corresponding to a given strength for the curved beam elements with variable curvatures is of fundamental importance in the design of these structures.

Until now, considerable researches on the in-plane free vibration of curved beams with variable curvatures have been performed. Tseng et al. (2000, 1997) and Huang et al. (1998b) studied the in-plane free

* Corresponding author. Tel.: +82-331-290-7514; fax: +82-331-290-7548.
E-mail address: kmye@yurim.skku.ac.kr (M.-Y. Kim).

0020-7683/03/$ - see front matter © 2003 Elsevier Science Ltd. All rights reserved.
doi:10.1016/S0020-7683(03)00113-6

vibration of arches with variable curvatures using the dynamic stiffness method based on Timoshenko beam theory. Oh et al. (2000, 1999) derived the governing equations of the in-plane free vibrations of non-circular arches. Tarnopolskaya et al. (1996) has reported the phenomenon of transformation of mode shapes with change in curvatures using the asymptotic analysis. And Gutierrez et al. (1989), Wang and Moore (1973), Wang (1972), Romanelli and Laura (1972) calculated the natural frequencies of non-circular arches. On the other hand, Huang et al. (2000, 1998a) investigated the out-of-plane free vibration behaviour and the linear dynamic response of non-circular curved beams using the Laplace transform and dynamic stiffness method. However most of these researches are confined to in-plane or out-of-plane vibration of non-circular curved beams with only symmetric cross-sections.

In case of spatial stability analysis of thin-walled circular curved beams, Timoshenko and Gere (1961) derived the governing equations for buckling of curved beams neglecting the effect of warping. Vlasov (1961) formulated the stability equations by substituting the curvature terms of the curved beam into the straight beam equilibrium equation. Usuki et al. (1979) developed a lateral–torsional buckling theory and finite element formulation of thin-walled circular arch accounting for prebuckling deflections. Also, Papangelis and Trahair (1987a,b) obtained analytical solutions for the lateral buckling of arch and compared them with experiment results. Yang and Kuo (1987) and Kuo and Yang (1991) presented a stability theory of symmetric thin-walled curved beam considering curvature effects and also, developed a straight beam element for buckling analysis of curved beams. Saleeb et al. (1992) developed a finite element model for the buckling analysis of shear flexible thin-walled frames using a mixed formulation. Kang and Yoo (1994a,b) derived analytical solutions for the stability behavior of simply supported thin-walled curved beams having a doubly symmetric open section. Chang et al. (1996) presented numerical solutions on spatial stability of the circular arch using the thin-walled straight beam element. Recently Kim et al. (2000a,b) developed a general theory for spatial stability analysis of non-symmetric thin-walled circular curved beams. However, though a great portion of the previous research has been conducted on the stability analysis of circular curved beams, to the authors' knowledge, the stability analysis of the curved beam with variable curvatures has rarely been studied.

In this paper, for spatially coupled free vibration and buckling of non-symmetric thin-walled curved beams with variable curvatures, an improved energy formulation is consistently presented based on the study of Kim et al. (2000a). Here the total potential energy of the non-circular curved beam is derived by introducing the displacement field considering both Vlasov's assumption and effects of variable curvatures and degenerating total potential energies for the elastic continuum to those for the curved beam. And then a thin-walled non-circular beam element for F.E. analysis is developed using the third-order Hermitian polynomials. Finally in order to illustrate the accuracy and the validity of this element, numerical solutions by this study are presented and compared with the results analyzed by ABAQUS' shell element (1992). In particular, the influences of the arch rise to span length ratio are investigated on spatial vibrational and buckling behaviors of non-circular beams with the parabolic and elliptic shapes.

2. Principle of linearized virtual work

The global coordinate system (x_1, x_2, x_3) of the thin-walled non-circular beam is shown in Fig. 1. The x_1-axis coincides with the centroidal axis which is curves in plane but x_2, x_3 are not necessarily principal inertia axes. This curvilinear coordinate is orthogonal if the cross-section is prismatic. Additional assumptions adopted in this study are

1. The thin-walled non-circular beam is linearly elastic and prismatic.
2. The cross-section is rigid with respect to in-plane deformation except for warping deformation.
3. The effects of shear deformations are negligible.

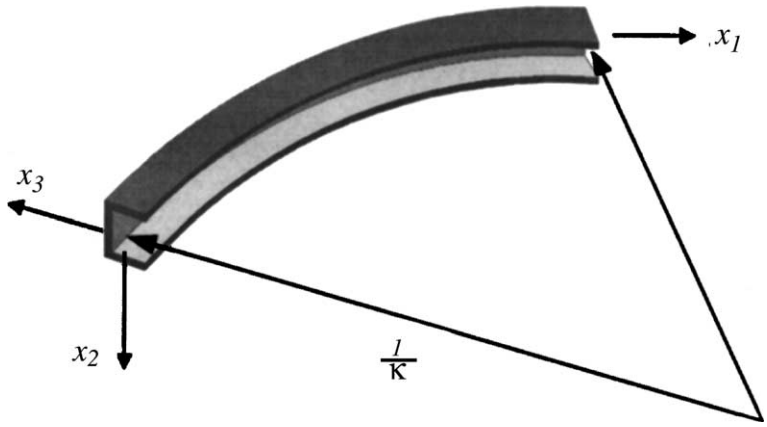

Fig. 1. Curvilinear coordinate system of a non-symmetric thin-walled curved beam.

For free vibration and buckling analysis of the general continuum, the principle of linearized virtual work is expressed as follows:

$$\int_V (\tau_{ij}\delta e_{ij} + {}^0\tau_{ij}\delta\eta_{ij} + {}^0\tau_{ij}\delta e^*_{ij})\,\mathrm{d}V - \omega^2 \int_V \rho U_i \delta U_i \,\mathrm{d}V = \int_S T_i \delta U_i \,\mathrm{d}S \tag{1}$$

where ${}^0\tau_{ij}$, τ_{ij} and e_{ij} are the initial, the incremental stress and the linear strain, respectively; η_{ij} and e^*_{ij} are the non-linear strain due to U_i and the linear strain due to U^*_i, respectively; ρ is the density; ω is the circular frequency; T_i is the surface force; U_i and U^*_i are linear and non-linear displacement components, respectively; δ denotes 'virtual'.

2.1. The displacement field for non-symmetric thin-walled cross-sections

Fig. 2 shows displacement parameters defined at the centroid along the x_1-axis of the non-symmetric thin-walled non-circular beam. e_2, e_3 are the position vector components of the shear center in the local coordinate. U_x, U_y, U_z and ω_1, ω_2, ω_3 are rigid body translations and rotations of the cross-section about x_1-, x_2- and x_3-axis, respectively. f is a warping parameter denoting the gradient of the twisting angle $\theta(=\omega_1)$ with respect to x_1-axis.

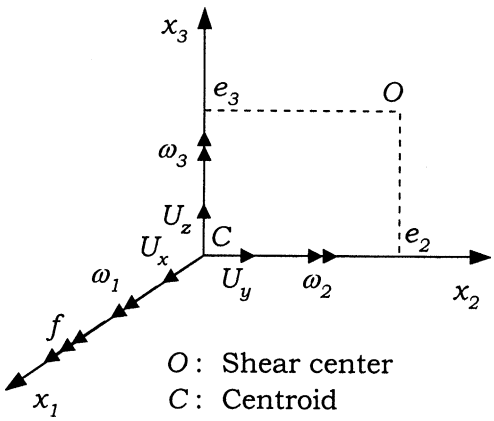

Fig. 2. Notation for displacement parameters.

From Frenet's formula (Love, 1934), rotational parameters ω_2, ω_3, f and an axial parameter g with respect to rigid body translations and twisting angle can be obtained by

$$\begin{aligned}\omega_2 &= -U_z' + \kappa U_x \\ \omega_3 &= U_y' \\ f &= -\theta' - \kappa U_y' \\ g &= U_x' + \kappa U_z\end{aligned} \tag{2a–d}$$

where differentiation with respect to x_1 is denoted by a prime and $\kappa(x_1)$ denotes the curvature of non-circular beams along the x_1-axis.

With the assumption that the cross-section is rigid with respect to cross-sectional in-plane deformation, the total displacement field including both the first and the second-order terms of rotational parameters can be expressed as follows (Kim et al., 2000a):

$$\boldsymbol{U} = \boldsymbol{U}_0 + \left(\boldsymbol{S} + \frac{1}{2}\boldsymbol{S}^2\right)\boldsymbol{X}_0 \tag{3}$$

where

$$\boldsymbol{U} = (U_1 + U_1^*, U_2 + U_2^*, U_3 + U_3^*)^{\mathrm{T}} \tag{4a}$$

$$\boldsymbol{U}_0 = (U_x + f\phi, U_y, U_z)^{\mathrm{T}} \tag{4b}$$

$$\boldsymbol{X}_0 = (0, x_2, x_3)^{\mathrm{T}} \tag{4c}$$

and

$$\boldsymbol{S} = \begin{bmatrix} 0 & -\omega_3 & \omega_2 \\ \omega_3 & 0 & -\omega_1 \\ -\omega_2 & \omega_1 & 0 \end{bmatrix} \tag{5}$$

where rotational components ω_1, ω_2, ω_3 should be interpreted to be semitangential rotations (Argyris and Symeonidis, 1981; Kim and Kim, 2000).

Substituting Eqs. (2), (4), and (5) into Eq. (3) and arranging in the component form, the displacement vector components of an arbitrary point on the thin-walled cross-section can be expressed as follows:

$$\begin{aligned}U_1 &= U_x - x_2 U_y' - x_3(U_z' - \kappa U_x) - (\theta' + \kappa U_y')\phi(x_2, x_3) \\ U_2 &= U_y - x_3\theta \\ U_3 &= U_z + x_2\theta\end{aligned} \tag{6a–c}$$

and

$$\begin{aligned}U_1^* &= \tfrac{1}{2}[-\theta(U_z' - \kappa U_x)x_2 + \theta U_y' x_3] \\ U_2^* &= \tfrac{1}{2}[-(\theta^2 + U_y'^2)x_2 - (U_z' - \kappa U_x)U_y' x_3] \\ U_3^* &= \tfrac{1}{2}[-(U_z' - \kappa U_x)U_y' x_2 - \{\theta^2 + (U_z' - \kappa U_x)^2\}x_3]\end{aligned} \tag{7a–c}$$

where U_i, U_i^* are displacement components corresponding to the first- and second-order terms of displacement parameters, respectively, while ϕ denotes the normalized warping function defined at the centroid. The kinematic relationship between ϕ and ϕ_s defined at the shear center is given by

$$\phi = \phi_s + e_2 x_3 - e_3 x_2 \tag{8}$$

Section properties used in this study are defined as follows:

$$
\begin{aligned}
&I_2 = \int_A x_3^2\,\mathrm{d}A, \quad I_3 = \int_A x_2^2\,\mathrm{d}A, \quad I_{23} = \int_A x_2x_3\,\mathrm{d}A,\\
&I_\phi = \int_A \phi^2\,\mathrm{d}A, \quad I_{\phi 2} = \int_A \phi x_3\,\mathrm{d}A, \quad I_{\phi 3} = \int_A \phi x_2\,\mathrm{d}A,\\
&I_{222} = \int_A x_3^3\,\mathrm{d}A, \quad I_{223} = \int_A x_2x_3^2\,\mathrm{d}A, \quad I_{233} = \int_A x_2^2x_3\,\mathrm{d}A,\\
&I_{333} = \int_A x_2^3\,\mathrm{d}A, \quad I_{\phi 22} = \int_A \phi x_3^2\,\mathrm{d}A, \quad I_{\phi 33} = \int_A \phi x_2^2\,\mathrm{d}A,\\
&I_{\phi 23} = \int_A \phi x_3x_2\,\mathrm{d}A, \quad I_{\phi\phi 2} = \int_A \phi^2x_3\,\mathrm{d}A, \quad I_{\phi\phi 3} = \int_A \phi^2x_2\,\mathrm{d}A
\end{aligned}
\tag{9}
$$

where A, I_2, I_3, I_{23} and I_ϕ are the cross-sectional area, the second moment of inertia about x_2- and x_3-axes, product moment of inertia and the warping moment of inertia, respectively. $I_{2\phi}(=I_2e_2)$ and $I_{3\phi}(=-I_3e_3)$ are product moments of inertia due to the normalized warping. $I_{ijk}(i,j,k=\phi,2,3)$ are the third moments of inertia. The transformation equations between section properties defined at the centroid–centroid axis and those at the centroid-shear center axis may be referred to Kim and Kim (2000).

On the other hand, stress resultants are defined as

$$
\begin{aligned}
&F_1 = \int_A \tau_{11}\,\mathrm{d}A, \quad F_2 = \int_A \tau_{12}\,\mathrm{d}A, \quad F_3 = \int_A \tau_{13}\,\mathrm{d}A\\
&M_1 = \int_A (\tau_{13}x_2 - \tau_{12}x_3)\,\mathrm{d}A, \quad M_2 = \int_A \tau_{11}x_3\,\mathrm{d}A, \quad M_3 = -\int_A \tau_{11}x_2\,\mathrm{d}A\\
&M_\phi = \int_A \tau_{11}\phi\,\mathrm{d}A, \quad M_p = \int_A \tau_{11}(x_2^2+x_3^2)\,\mathrm{d}A
\end{aligned}
\tag{10a–h}
$$

where F_1, F_2 and F_3 are an axial force and shear forces, respectively; M_2 and M_3 are bending moments with respect to x_2- and x_3-axes, respectively; M_1 and M_ϕ are the total twisting moment and the bimoment with respect to the x_1-axis, respectively; M_p is a stress resultant known as the Wagner effect.

2.2. Strain–displacement and force–deformation relations

According to the assumption of rigid deformation with respect to the in-plane, the in-plane strains (e_{22}, e_{33}, e_{23}) are negligible. For the thin-walled curved beam, a complete set of linear strain–displacement relations due to the first-order displacement parameters are expressed as follows:

$$
\begin{aligned}
e_{11} &= (U_{1,1} + \kappa U_3)\left(\frac{1}{1+\kappa x_3}\right)\\
&= [U_x' + \kappa U_z - x_2(U_y'' - \kappa\theta) - x_3(U_z'' - \kappa U_x') - \phi(\theta'' + \kappa U_y'')]\frac{1}{1+\kappa x_3}
\end{aligned}
\tag{11a}
$$

$$
2e_{12} = U_{2,1}\left(\frac{1}{1+\kappa x_3}\right) + U_{1,2} = -x_3(\theta' + \kappa U_y')\frac{1}{1+\kappa x_3} - (\theta' + \kappa U_y')\phi_{,2}
\tag{11b}
$$

$$
2e_{13} = (U_{3,1} - \kappa U_1)\left(\frac{1}{1+\kappa x_3}\right) + U_{1,3} = (x_2 + \kappa\phi)(\theta' + \kappa U_y')\frac{1}{1+\kappa x_3} - (\theta' + \kappa U_y')\phi_{,3}
\tag{11c}
$$

where the subscript 'comma' indicates partial differentiation with respect to the curvilinear coordinate (x_1, x_2, x_3). It should be noticed that Eqs. (11b) and (11c) represent only shear strains due to Saint-Venant torsion because $\theta' + \kappa U_y'$ means the derivative of a twisting angle considering the curvature effect. Consequently, it means that shear deformations due to shear forces and the restrained torsion vanish.

Substituting Eq. (11a) into Eqs. (10a), (e)–(g) and integrating over the cross-section yield the following force–deformation relations.

$$\begin{pmatrix} F_1 \\ M_2 \\ M_3 \\ M_\phi \end{pmatrix} = E \begin{bmatrix} \widehat{A} & -\kappa\widehat{I_2} & \kappa\widehat{I_{23}} & -\kappa\widehat{I_{\phi 2}} \\ -\kappa\widehat{I_2} & \widehat{I_2} & -\widehat{I_{23}} & \widehat{I_{\phi 2}} \\ \kappa\widehat{I_{23}} & -\widehat{I_{23}} & \widehat{I_3} & -\widehat{I_{\phi 3}} \\ -\kappa\widehat{I_{\phi 2}} & \widehat{I_{\phi 2}} & -\widehat{I_{\phi 3}} & \widehat{I_\phi} \end{bmatrix} \begin{pmatrix} U_x' + \kappa U_z \\ (-U_z' + \kappa U_x)' \\ U_y'' - \kappa\theta \\ -(\theta' + \kappa U_y)' \end{pmatrix} \tag{12}$$

where $\widehat{A} = A + \kappa^2 \widehat{I_2}$. An approximation is used to account for the thickness-curvature effect as follows:

$$\frac{1}{1+\kappa x_3} \simeq 1 - \kappa x_3 + \kappa^2 x_3^2 \tag{13}$$

On the other hand, non-linear strain–displacement relations due to first-order displacement parameters and linear relations due to the second-order rotation parameters are expressed in Eqs. (14) and (15), respectively.

$$\eta_{11} = \frac{1}{2}[(U_{1,1} + \kappa U_3)^2 + U_{2,1}^2 + (U_{3,1} - \kappa U_1)^2]\left(\frac{1}{1+\kappa x_3}\right)^2 \tag{14a}$$

$$\eta_{12} = \frac{1}{2}[U_{1,2}(U_{1,1} + \kappa U_3) + U_{2,2} \cdot U_{2,1} + U_{3,2}(U_{3,1} - \kappa U_1)]\frac{1}{1+\kappa x_3} \tag{14b}$$

$$\eta_{13} = \frac{1}{2}[U_{1,3}(U_{1,1} + \kappa U_3) + U_{2,3} \cdot U_{2,1} + U_{3,3}(U_{3,1} - \kappa U_1)]\frac{1}{1+\kappa x_3} \tag{14c}$$

and

$$e_{11}^* = (U_{1,1}^* + \kappa U_3^*)\frac{1}{1+\kappa x_3} \tag{15a}$$

$$2e_{12}^* = U_{2,1}^*\frac{1}{1+\kappa x_3} + U_{1,2}^* \tag{15b}$$

$$2e_{13}^* = (U_{3,1}^* - \kappa U_1^*)\frac{1}{1+\kappa x_3} + U_{1,3}^* \tag{15c}$$

2.3. Total potential energy of thin-walled curved beams with variable curvatures

Total potential energy Π of thin-walled curved beams with variable curvatures consists of the elastic strain energy Π_E, the potential energy $\Pi_G (= \Pi_{G1} + \Pi_{G2})$ due to initial stresses and the kinetic energy T as follows:

$$\Pi = \Pi_E + \Pi_{G1} + \Pi_{G2} - T \tag{16a}$$

where

$$\Pi_E = \frac{1}{2}\int_0^l \int_A [\tau_{11}e_{11} + 2\tau_{12}e_{12} + 2\tau_{13}e_{13}](1+\kappa x_3)\,\mathrm{d}A\,\mathrm{d}x_1 \tag{16b}$$

$$\Pi_{G1} = \int_0^l \int_A [{}^0\tau_{11}\eta_{11} + 2{}^0\tau_{12}\eta_{12} + 2{}^0\tau_{13}\eta_{13}](1+\kappa x_3)\,\mathrm{d}A\,\mathrm{d}x_1 \tag{16c}$$

$$\Pi_{G2} = \int_0^l \int_A [{}^0\tau_{11}e^*_{11} + 2{}^0\tau_{12}e^*_{12} + 2{}^0\tau_{13}e^*_{13}](1+\kappa x_3)\,\mathrm{d}A\,\mathrm{d}x_1 \tag{16d}$$

$$T = \frac{1}{2}\rho\omega^2 \int_0^l \int_A [U_1^2 + U_2^2 + U_3^2](1+\kappa x_3)\,\mathrm{d}A\,\mathrm{d}x_1 \tag{16e}$$

where l, E and G are the length of curved beams, Young's modulus and shear modulus, respectively.

Substituting Eq. (11) into Eq. (16b) and integrating over the cross-sectional area yields:

$$\begin{aligned}\Pi_E = \frac{1}{2}\int_0^L &[F_1(U_x' + \kappa U_z) + M_2(-U_z' + \kappa U_x)' + M_3(U_y'' - \kappa\theta) - M_\phi(\theta' + \kappa U_y')' \\ &+ (M_1 - M_R)(\theta' + \kappa U_y')]\,\mathrm{d}x_1\end{aligned} \tag{17a}$$

where

$$M_R = \int_A \{(\tau_{12}\phi_{,2} + \tau_{13}\phi_{,3})(1+\kappa x_3) - \tau_{13}\kappa\phi\}\,\mathrm{d}A. \tag{17b}$$

Now substituting the force–deformation relations (12) into the elastic strain energy (17a) leads to

$$\begin{aligned}\Pi_E = \frac{1}{2}\int_0^L \Big[&E(A + \underline{\kappa^2\widehat{I_2}})(U_x' + \kappa U_z)^2 + E\widehat{I_3}(U_y'' - \kappa\theta)^2 + \underline{E\widehat{I_2}\{U_z'' - (\kappa U_x)'\}^2} \\ &+ \underline{2E\widehat{I_2}\kappa(U_x' + \kappa U_z)\{U_z'' - (\kappa U_x)'\}} + 2E\widehat{I_{\phi 3}}(U_y'' - \kappa\theta)(\theta'' + \kappa' U_y' + \kappa U_y'') + E\widehat{I_\phi}(\theta'' + \kappa' U_y' + \kappa U_y'')^2 \\ &+ GJ(\theta' + \kappa U_y')^2 + \underline{2E\widehat{I_{23}}(U_y'' - \kappa\theta)\{U_z'' - (\kappa U_x)'\}} + \underline{2E\widehat{I_{23}}\kappa(U_y'' - \kappa\theta)(U_x' + \kappa U_z)} \\ &+ \underline{2E\widehat{I_{\phi 2}}(\theta'' + \kappa' U_y' + \kappa U_y'')\{U_z'' - (\kappa U_x)'\}} + \underline{2E\widehat{I_{\phi 2}}(\theta'' + \kappa' U_y' + \kappa U_y'')(U_x' + \kappa U_z)}\Big]\,\mathrm{d}x_1\end{aligned} \tag{18}$$

Then simplifying the underlined terms in Eq. (18), Π_E may be obtained as follows:

$$\begin{aligned}\Pi_E = \frac{1}{2}\int_0^L \Big[&EA(U_x' + \kappa U_z)^2 + E\widehat{I_3}(U_y'' - \kappa\theta)^2 + E\widehat{I_2}(U_z'' + \kappa^2 U_z - \kappa' U_x)^2 + E\widehat{I_\phi}(\theta'' + \kappa' U_y' + \kappa U_y'')^2 \\ &+ 2E\widehat{I_{\phi 3}}(U_y'' - \kappa\theta)(\theta'' + \kappa' U_y' + \kappa U_y'') + GJ(\theta' + \kappa U_y')^2 + 2E\widehat{I_{23}}(U_y'' - \kappa\theta)(U_z'' + \kappa^2 U_z - \kappa' U_x) \\ &+ 2E\widehat{I_{\phi 2}}(\theta'' + \kappa' U_y' + \kappa U_y'')(U_z'' + \kappa^2 U_z - \kappa' U_x)\Big]\,\mathrm{d}x_1\end{aligned} \tag{19a}$$

where

$$\begin{aligned}&\widehat{I_2} = I_2 - \kappa I_{222}, \quad \widehat{I_3} = I_3 - \kappa I_{233}, \quad \widehat{I_{23}} = I_{23} - \kappa I_{223} \\ &\widehat{I_\phi} = I_\phi - \kappa I_{\phi\phi 2}, \quad \widehat{I_{\phi 2}} = I_{\phi 2} - \kappa I_{\phi 22}, \quad \widehat{I_{\phi 3}} = I_{\phi 3} - \kappa I_{\phi 23}\end{aligned} \tag{19b}$$

and J is the torsional constant, and the following relation is used:

$$M_1 - M_R = M_1 - M_\phi' = GJ(\theta' + \kappa U_y') \tag{20}$$

Next, substituting the strain–displacement relations into Eqs. (16c) and (16d), noting the definition of Eq. (10), and considering the thickness-curvature effect of Eq. (13), Π_{G1} and Π_{G2} are expressed, respectively, as follows:

$$\begin{aligned}\Pi_{G1} = \frac{1}{2}\int_0^L \Big[& {}^0F_1\{U_y'^2 + (U_z' - \kappa U_x)^2\} + {}^0M_2\{-2U_y'\theta' - \kappa U_y'^2 + \underline{\kappa(U_z' - \kappa U_x)^2}\} \\ & - 2{}^0M_3(U_z' - \kappa U_x)(\theta' + \kappa U_y') + 2{}^0F_2\theta(U_z' - \kappa U_x) - 2{}^0F_3U_y'\theta \\ & + 2\int_A {}^0\tau_{12}x_3\,\mathrm{d}A\{U_y'(U_z' - \kappa U_x)' + \kappa\theta(U_z' - \kappa U_x)\} + 2\int_A {}^0\tau_{13}x_2\,\mathrm{d}A(U_z' - \kappa U_x)(U_y'' - \kappa\theta) \\ & \underline{+2\int_A {}^0\tau_{12}x_2\,\mathrm{d}A\{U_y'(U_y'' - \kappa\theta) + \theta(\theta' + \kappa U_y')\} + 2\int_A {}^0\tau_{13}x_3\,\mathrm{d}A\{(U_z' - \kappa U_x)(U_z' - \kappa U_x)' + \theta\theta'\}} \\ & + {}^0M_p(\theta' + \kappa U_y')^2 + 2\kappa{}^0M_\phi(U_z' - \kappa U_x)(\theta' + \kappa U_y')\Big]\mathrm{d}x_1 \end{aligned} \tag{21}$$

and

$$\begin{aligned}\Pi_{G2} = \frac{1}{2}\int_0^L \Big[& {}^0M_3\{\{\theta(U_z' - \kappa U_x)\}' + \kappa U_y'(U_z' - \kappa U_x)\} + {}^0M_2\{(\theta U_y')' - \kappa\theta^2 - \underline{\kappa(U_z' - \kappa U_x)^2}\} \\ & - {}^0F_2\theta(U_z' - \kappa U_x) + {}^0F_3(\theta U_y') \underline{- \int_A {}^0\tau_{12}x_2\,\mathrm{d}A(\theta^2 + U_y'^2)'} - \int_A {}^0\tau_{12}x_3\,\mathrm{d}A\{\{U_y'(U_z' - \kappa U_x)\}' \\ & + \kappa\theta(U_z' - \kappa U_x)\} - \int_A {}^0\tau_{13}x_2\,\mathrm{d}A\{\{U_y'(U_z' - \kappa U_x)\}' + \kappa\theta(U_z' - \kappa U_x)\} \\ & \underline{- \int_A {}^0\tau_{13}x_3\,\mathrm{d}A\{\theta^2 + (U_z' - \kappa U_x)^2\}'}\Big]\mathrm{d}x_1 \end{aligned} \tag{22}$$

where it should be noted that underlined terms existing in Eqs. (21) and (22) cancel out naturally and energy terms due to the total torque M_1 are obtained without introduction of awkward assumptions (see Eq. (25)). Also, the inextensibility condition (23) is utilized.

$$U_x' + \kappa U_z \simeq 0 \tag{23}$$

Consequently, summing up Eqs. (21) and (22), the final expression for the potential energy functional Π_G is represented as follows:

$$\begin{aligned}\Pi_G = \frac{1}{2}\int_0^L \big[& {}^0F_1\{U_y'^2 + (U_z' - \kappa U_x)^2\} + {}^0M_p(\theta' + \kappa U_y')^2 - {}^0F_3(U_y'\theta) + {}^0M_2\{(U_y'' - \kappa\theta)\theta - U_y'(\theta' + \kappa U_y')\} \\ & + 2\kappa{}^0M_\phi(U_z' - \kappa U_x)(\theta' + \kappa U_y') + {}^0M_3\{(U_z' - \kappa U_x)'\theta - (U_z' - \kappa U_x)(\theta' + \kappa U_y')\} + {}^0F_2\theta(U_z' - \kappa U_x) \\ & + {}^0M_1\{(U_z' - \kappa U_x)(U_y'' - \kappa\theta) - U_y'(U_z' - \kappa U_x)'\}\big]\mathrm{d}x_1 \end{aligned} \tag{24}$$

Here to investigate effects of the second-order terms of finite semitangential rotations, we assume that the underlined terms may be neglected in Eq. (21) and Eq. (25) is valid for the torsional moment (see Argyris et al., 1979; Kim et al., 2001).

$$0.5{}^0M_1 = \int_A {}^0\tau_{13}x_2\,\mathrm{d}A = -\int_A {}^0\tau_{12}x_3\,\mathrm{d}A \tag{25}$$

Then the potential energy Π_{G1} including only the first-order term of finite rotations may be written as follows:

$$\Pi_{G1} = \frac{1}{2}\int_0^L [{}^0F_1\{U_y'^2 + (U_z' - \kappa U_x)^2\} + {}^0M_2(-2U_y'\theta' - \kappa U_y'^2) - 2^0M_3(U_z' - \kappa U_x)(\theta' + \kappa U_y') + 2^0F_2\theta(U_z' - \kappa U_x) - 2^0F_3U_y'\theta + {}^0M_p(\theta' + \kappa U_y')^2 + {}^0M_1\{(U_z' - \kappa U_x)(U_y'' - 2\kappa\theta) - U_y'(U_z' - \kappa U_x)'\} + 2\kappa^0M_\phi(U_z' - \kappa U_x)(\theta' + \kappa U_y')]\,dx_1 \tag{26}$$

For the spatial stability analysis of non-symmetric curved beams subjected to general loadings, the stress resultant M_p denoting Wagner effect should be expressed with respect to stress resultants F_1, M_2, M_3, M_ϕ as follows:

$$M_p = \beta_1 F_1 + \beta_2 M_2 + \beta_3 M_3 + \beta_\phi M_\phi \tag{27}$$

Now to evaluate coefficients $\beta_1, \beta_2, \beta_3, \beta_\phi$, substituting Eq. (11a) into Eq. (10h) and integrating over the cross-section leads to

$$M_p = E\langle \widehat{I_2} + \widehat{I_3}, I_{222} + I_{233}, -I_{223} - I_{333}, I_{\phi 22} + I_{\phi 33}\rangle \begin{pmatrix} U_x' + \kappa U_z \\ (-U_z' + \kappa U_x)' \\ U_y'' - \kappa\theta \\ -(\theta' + \kappa U_y)' \end{pmatrix} \tag{28}$$

Then substituting force–deformation relations (12) into Eq. (27) and comparing the result with Eq. (28), four coefficients are determined as follows:

$$\begin{bmatrix} \widehat{A} & -\kappa\widehat{I_2} & \kappa\widehat{I_{23}} & -\kappa\widehat{I_{\phi 2}} \\ -\kappa\widehat{I_2} & \widehat{I_2} & -\widehat{I_{23}} & \widehat{I_{\phi 2}} \\ \kappa\widehat{I_{23}} & -\widehat{I_{23}} & \widehat{I_3} & -\widehat{I_{\phi 3}} \\ -\kappa\widehat{I_{\phi 2}} & \widehat{I_{\phi 2}} & -\widehat{I_{\phi 3}} & \widehat{I_\phi} \end{bmatrix} \begin{pmatrix} \beta_1 \\ \beta_2 \\ \beta_3 \\ \beta_\phi \end{pmatrix} = \begin{pmatrix} \widehat{I_2} + \widehat{I_3} \\ I_{233} + I_{222} \\ -I_{333} - I_{223} \\ I_{33\phi} + I_{22\phi} \end{pmatrix} \tag{29}$$

Finally in order to obtain the kinetic energy T relevant to the non-symmetric cross-section, substituting the displacement components Eq. (6) into Eq. (16e) and integrating it over the cross-section yields

$$T = \frac{1}{2}\rho\omega^2\int_0^L \Big[A(U_x^2 + U_y^2 + U_z^2) + \widetilde{I_0}\theta^2 + \widetilde{I_3}U_y'^2 + \widetilde{I_2}(U_z' - \kappa U_x)^2 + \widetilde{I_\phi}(\theta' + \kappa U_y')^2 + 2\widetilde{I_{\phi 3}}U_y'(\theta' + \kappa U_y') + 2\widetilde{I_{\phi 2}}(U_z' - \kappa U_x)(\theta' + \kappa U_y') - 2\kappa I_{\phi 2}U_x(\theta' + \kappa U_y') - 2\kappa I_2(U_y\theta) - 2\kappa I_2U_x(U_z' - \kappa U_x) + 2\kappa I_{223}U_y'(U_z' - \kappa U_x) + 2I_{23}(U_y'U_z' - 2\kappa U_xU_y' + \kappa U_z\theta)\Big]\,dx_1 \tag{30a}$$

where

$$\begin{aligned} &\widetilde{I_2} = I_2 + \kappa I_{222}, \quad \widetilde{I_3} = I_3 + \kappa I_{233}, \quad \widetilde{I_\phi} = I_\phi + \kappa I_{\phi\phi 2}, \quad \widetilde{I_{\phi 2}} = I_{\phi 2} + \kappa I_{\phi 22} \\ &\widetilde{I_{\phi 3}} = I_{\phi 3} + \kappa I_{\phi 23}, \quad I_0 = I_2 + I_3, \quad \widetilde{I_0} = I_0 + \kappa(I_{222} + I_{233}) \end{aligned} \tag{30b}$$

3. The thin-walled non-circular beam element

For F.E. analysis of non-circular beams, a thin-walled curved beam element with the non-symmetric cross-section is developed in this section. Fig. 3 shows the nodal displacement vector of a thin-walled curved beam element including restrained warping effects. In order to accurately express the deformation of element, it is necessary to use pertinent shape functions.

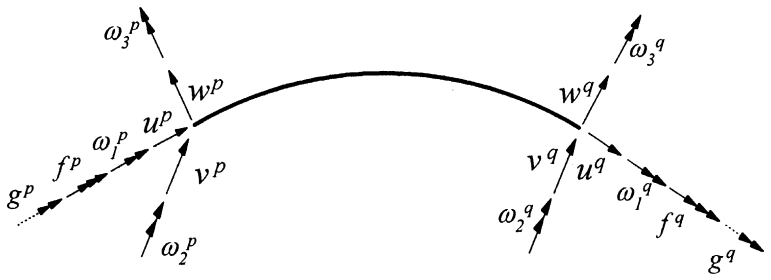

Fig. 3. Nodal displacement vector of a thin-walled curved beam element.

In this study, cubic Hermitian polynomials are adopted to interpolate displacement parameters that are defined at the centroid axis. Thus this curved element has two nodes and eight nodal degrees of freedom per node. As a result, the element displacement parameters U_x, U_y, U_z, θ can be interpolated with respect to the nodal displacements as follows:

$$U_x = h_1 \cdot u^p + h_2 \cdot g^p + h_3 \cdot u^q + h_4 \cdot g^q \tag{31a}$$

$$U_y = h_1 \cdot v^p + h_2 \cdot \omega_3^p + h_3 \cdot v^q + h_4 \cdot \omega_3^q \tag{31b}$$

$$U_z = h_1 \cdot w^p - h_2 \cdot \omega_2^p + h_3 \cdot w^q - h_4 \cdot \omega_2^q \tag{31c}$$

$$\theta = h_1 \cdot \omega_1^p - h_2 \cdot f^p + h_3 \cdot \omega_1^q - h_4 \cdot f^q \tag{31d}$$

where

$$u^p = U_x(0), \quad v^p = U_y(0), \quad w^p = U_z(0) \tag{32a–c}$$

$$\omega_1^p = \theta(0), \quad \omega_2^p = -U_z'(0), \quad \omega_3^p = U_y'(0) \tag{32d–f}$$

$$f^p = -\theta'(0), \quad g^p = U_x'(0) \tag{32g, h}$$

and h_i denotes cubic Hermitian polynomials.

Substituting the shape functions, material and cross-sectional properties and distribution of internal forces into Eqs. (19), (24) and (30) and integrating along the element length, the equilibrium equation of thin-walled curved beam element are obtained in matrix form as following:

$$(K_e + K_g)U_e - \omega^2 M_e U_e = F_e \tag{33}$$

and

$$U_e = \langle u^p, v^p, w^p, \omega_1^p, \omega_2^p, \omega_3^p, f^p, g^p, u^q, v^q, w^q, \omega_1^q, \omega_2^q, \omega_3^q, f^q, g^q \rangle \tag{34a}$$

$$F_e = \langle F_1^p, F_2^p, F_3^p, M_1^p, M_2^p, M_3^p, M_\phi^p, F_m^p, F_1^q, F_2^q, F_3^q, M_1^q, M_2^q, M_3^q, M_\phi^q, F_m^q \rangle \tag{34b}$$

where K_e, K_g and M_e denote 16×16 element elastic and geometric stiffness and mass matrices, respectively, which are evaluated using Gauss five-point numerical integration scheme. U_e and F_e are nodal displacement and force vectors, respectively. Here it is convenient to introduce rotational and axial nodal displacement components considering curvature effect as follows:

$$\widehat{\omega_2^p} = -U_z'(0) + \kappa U_x(0) = \omega_2^p + \kappa u^p \tag{35a}$$

$$\widehat{f^p} = -\theta'(0) - \kappa U_y'(0) = f^p - \kappa\omega_3^p \tag{35b}$$

$$\widehat{g^p} = U_x'(0) + \kappa U_z(0) = g^p + \kappa w^p \tag{35c}$$

In order to evaluate the element matrices corresponding to the newly defined nodal displacement components, the transformation equation between the nodal displacement vector U_e and the new displacement vector $\widehat{U_e}$ considering the effect of curvature may be obtained from Eq. (35) as follows:

$$U_\alpha = T_1 \widehat{U_\alpha}, \quad \alpha = p, q \tag{36}$$

where

$$U_\alpha^{\mathrm{T}} = \{\, u^\alpha \quad v^\alpha \quad w^\alpha \quad \omega_1^\alpha \quad \omega_2^\alpha \quad \omega_3^\alpha \quad f^\alpha \quad g^\alpha \,\}, \quad \widehat{U_\alpha}^{\mathrm{T}} = \{\, u^\alpha \quad v^\alpha \quad w^\alpha \quad \omega_1^\alpha \quad \widehat{\omega_2^\alpha} \quad \omega_3^\alpha \quad \widehat{f^\alpha} \quad \widehat{g^\alpha} \,\} \tag{37a, b}$$

and

$$T_1 = \left[\begin{array}{cccc:cccc} 1.0 & \cdot & \cdot & \cdot & \cdot & \cdot & \cdot & \cdot \\ \cdot & 1.0 & \cdot & \cdot & \cdot & \cdot & \cdot & \cdot \\ \cdot & \cdot & 1.0 & \cdot & \cdot & \cdot & \cdot & \cdot \\ \cdot & \cdot & \cdot & 1.0 & \cdot & \cdot & \cdot & \cdot \\ \hdashline -\chi & \cdot & \cdot & \cdot & 1.0 & \cdot & \cdot & \cdot \\ \cdot & \cdot & \cdot & \cdot & \cdot & 1.0 & \cdot & \cdot \\ \cdot & \cdot & \cdot & \cdot & \cdot & \chi & 1.0 & \cdot \\ \cdot & \cdot & -\chi & \cdot & \cdot & \cdot & \cdot & 1.0 \end{array}\right] \tag{38}$$

Now using Eq. (38), Eq. (33) is transformed to

$$(\widehat{K_e} + \widehat{K_g})\widehat{U_e} - \omega^2 \widehat{M_e}\widehat{U_e} = \widehat{F_e} \tag{39}$$

where

$$\widehat{U_e} = \left\langle u^p, v^p, w^p, \omega_1^p, \widehat{\omega_2^p}, \omega_3^p, \widehat{f^p}, \widehat{g^p}, u^q, v^q, w^q, \omega_1^q, \widehat{\omega_2^q}, \omega_3^q, \widehat{f^q}, \widehat{g^q} \right\rangle \tag{40a}$$

$$\widehat{F_e} = \left\langle F_1^p, F_2^p, F_3^p, M_1^p, \widehat{M_2^p}, M_3^p, \widehat{M_\phi^p}, \widehat{F_m^p}, F_1^q, F_2^q, F_3^q, M_1^q, \widehat{M_2^q}, M_3^q, \widehat{M_\phi^q}, \widehat{F_m^q} \right\rangle \tag{40b}$$

and matrices and vectors in Eq. (39) are evaluated as follows:

$$\widehat{K_e} = T^{\mathrm{T}} K_e T, \quad U_e = T\widehat{U_e}, \quad \widehat{F_e} = T^{\mathrm{T}} F_e \tag{41a}$$

where

$$T = \left[\begin{array}{c:c} T_1 & \cdot \\ \hdashline \cdot & T_1 \end{array}\right] \tag{41b}$$

Lastly using direct stiffness method, the matrix equilibrium equation for the free vibration and elastic spatial buckling analysis of non-symmetric thin-walled curved beam with variable curvature is obtained as

$$[K_{\mathrm{E}} + \lambda K_{\mathrm{G}}]U - \omega^2 MU = F \tag{42}$$

where M, K_E and K_G are global mass, global elastic and geometric stiffness matrices, respectively; F denotes the global nodal force vector and becomes zero vector for free vibration and stability analysis and λ denotes the load parameter under the assumption of proportional loading; and K_G is calculated for a predefined initial stress distribution corresponding to the prebuckling loading state.

4. Numerical examples

The total potential energy has been derived and F.E. procedures have been developed for spatial free vibration and stability analysis of non-symmetric thin-walled curved beams with variable curvatures. In this section, spatial free vibration and stability analysis for curved beams of the parabolic and elliptic geometries with clamped–clamped and clamped–free end constraints are performed according to the variation of arch rise to span length ratio.

4.1. Convergence study

Figs. 4 and 5 show the geometric configuration of parabolic and elliptic arches having the same span length l and rise h and their channel cross-sections monosymmetric with respect to x_2- and x_3-axis, respectively. To examine the convergence property of the thin-walled curved beams with variable curvatures developed by this study, spatial free vibration and stability analysis for curved beams of the parabolic with clamped–free end constraints are performed. The cross-section of curved beam is monosymmetric with respect to x_3-axis and the arch rise to span length ratio (h/l) is 0.4.

The in-plane and out-of-plane natural frequencies and the lateral buckling load normalized with respect to the F.E. solution using 30 curved beam elements are presented in Figs. 6 and 7 as the element number increases. From Fig. 6, it can be found that the convergence speed of natural frequencies for out-of-plane modes is higher than that for in-plane modes. Also, Figs. 6 and 7 show that the convergence speed is fast

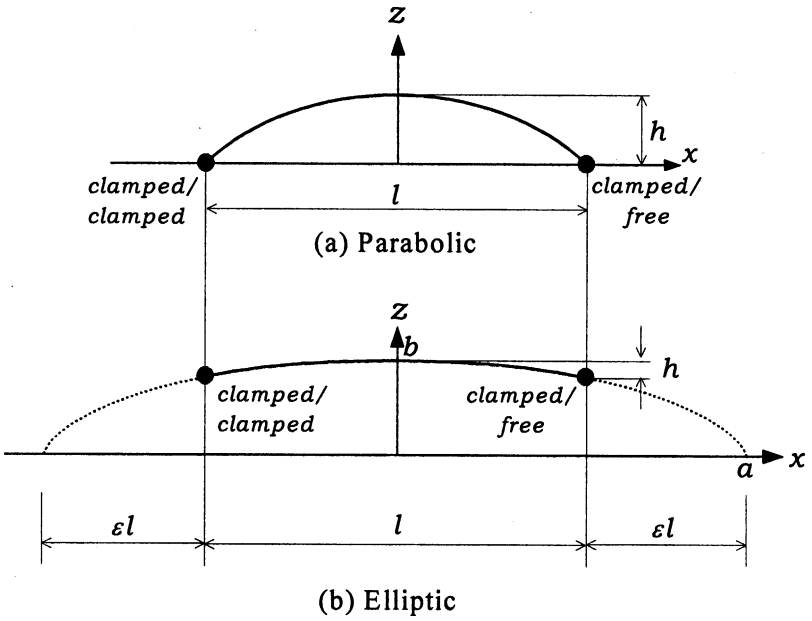

Fig. 4. Shapes and boundary conditions of arches for vibration analysis.

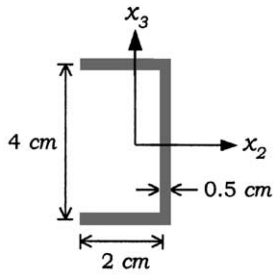

(a) Cross section of monosymmetric with respect to x_2 axis

$A = 4.0\,cm^2$, $E = 30{,}000\,kg/cm^2$, $G = 11{,}500\,kg/cm^2$, $J = 0.33333\,cm^4$, $e_2 = 1.25\,cm$, $e_3 = 0.0\,cm$, $I_2 = 10.66667\,cm^4$, $I_3 = 1.66667\,cm^4$, $I_{222} = 0.0\,cm^5$, $I_{223} = -2.66667\,cm^5$, $I_{233} = 0.0\,cm^5$, $I_{333} = -1.0\,cm^5$, $I_\phi = 21.33333\,cm^6$, $I_{\phi 2} = 13.33333\,cm^5$, $I_{\phi 3} = 0.0\,cm^5$, $I_{\phi 22} = 0.0\,cm^6$, $I_{\phi 23} = -8.0\,cm^6$, $I_{\phi 33} = 0.0\,cm^6$, $I_{\phi\phi 2} = 0.0\,cm^7$, $I_{\phi\phi 3} = -18.0\,cm^7$

(b) Material and section properties of monosymmetric with respect to x_2 axis

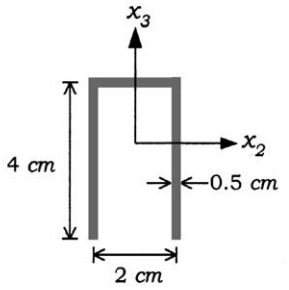

(c) Cross section of monosymmetric with respect to x_3 axis

$A = 5.0\,cm^2$, $E = 30{,}000\,kg/cm^2$, $G = 11{,}500\,kg/cm^2$, $J = 0.41667\,cm^4$, $e_2 = 0.0\,cm$, $e_3 = 3.44615\,cm$, $I_2 = 8.53333\,cm^4$, $I_3 = 4.33333\,cm^4$, $I_{222} = -2.56\,cm^5$, $I_{223} = 0.0\,cm^5$, $I_{233} = -1.06667\,cm^5$, $I_{333} = 0.0\,cm^5$, $I_\phi = 58.02667\,cm^6$, $I_{\phi 2} = 0.0\,cm^5$, $I_{\phi 3} = -14.93333\,cm^5$, $I_{\phi 22} = 0.0\,cm^6$, $I_{\phi 23} = 10.24\,cm^6$, $I_{\phi 33} = 0.0\,cm^6$, $I_{\phi\phi 2} = -59.904\,cm^7$, $I_{\phi\phi 3} = 0.0\,cm^7$

(d) Material and section properties of monosymmetric with respect to x_3 axis

Fig. 5. Monosymmetric cross-sections.

and results by 20 curved beam elements give accurate solutions. Accordingly, in subsequent examples on the free vibration and buckling problems of non-circular curved beam, an entire beam is modeled using 20 curved beam elements.

4.2. Free vibration of thin-walled curved beams

The clamped–clamped and clamped–free end constraints are considered (see Fig. 4). The influence of rise to span length ratio of arch is investigated for two types of arches. In this example, 20 curved beam

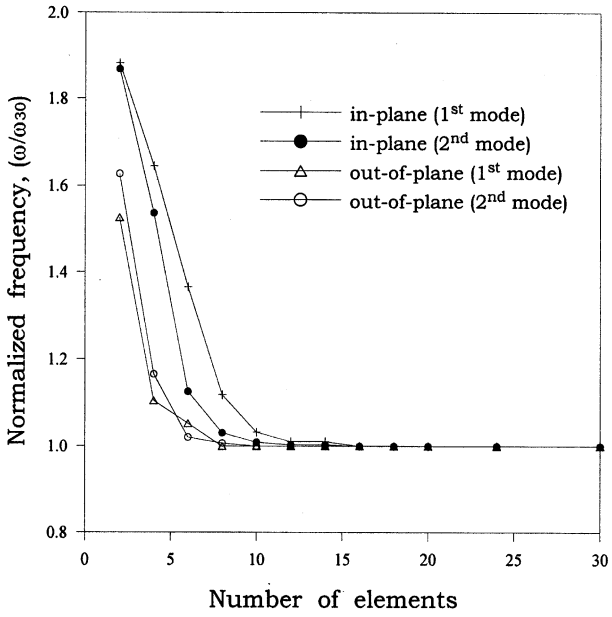

Fig. 6. Convergence of normalized frequencies.

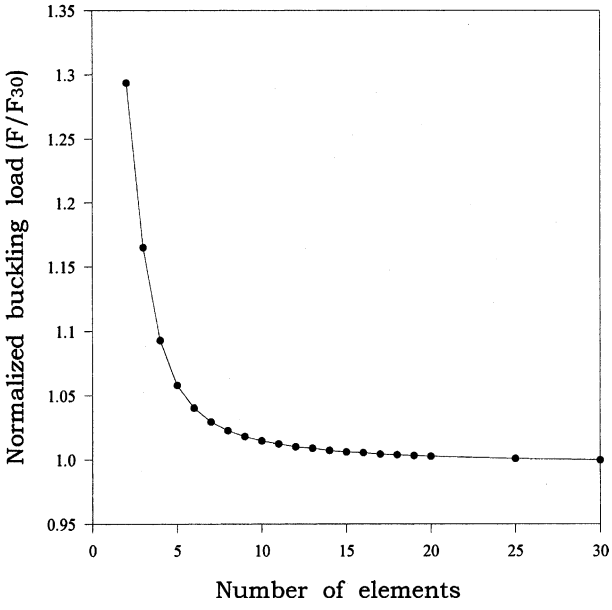

Fig. 7. Convergence of normalized buckling load.

elements and 320 and 400 shell elements are used for analysis of arches monosymmetric with respect to x_2- and x_3-axis, respectively.

Tables 1 and 2 show natural frequencies of parabolic and elliptic arches monosymmetric with respect to x_2-axis that have spatially coupled mode shapes. On the other hand, mode shapes of arches monosymmetric

Table 1
Natural frequencies for clamped–clamped arch with monosymmetric section x_2-axis (rad/s)

Shape		Parabolic		Elliptic	
h/l	Mode	Present study	ABAQUS	Present study	ABAQUS
0.2	1	0.310	0.312	0.310	0.312
	2	0.883	0.886	0.879	0.883
	3	1.828	1.834	1.817	1.823
	4	2.275	2.254	2.262	2.241
	5	3.121	3.130	3.102	3.110
	6	4.111	4.060	4.039	3.986
0.3	1	0.237	0.239	0.236	0.238
	2	0.668	0.669	0.663	0.664
	3	1.419	1.421	1.406	1.408
	4	1.792	1.781	1.774	1.761
	5	2.469	2.473	2.449	2.452
	6	3.572	3.532	3.538	3.496
0.4	1	0.183	0.184	0.182	0.183
	2	0.509	0.509	0.503	0.503
	3	1.098	1.099	1.085	1.086
	4	1.378	1.379	1.359	1.359
	5	1.930	1.933	1.913	1.915
	6	2.896	2.878	2.886	2.868

Table 2
Natural frequencies for clamped–free arch with monosymmetric section x_2-axis (rad/s)

Shape		Parabolic		Elliptic	
h/l	Mode	Present study	ABAQUS	Present study	ABAQUS
0.2	1	0.035	0.034	0.035	0.034
	2	0.156	0.156	0.155	0.155
	3	0.203	0.203	0.203	0.202
	4	0.727	0.723	0.718	0.715
	5	0.768	0.766	0.761	0.759
	6	1.677	1.676	1.642	1.640
0.3	1	0.025	0.024	0.024	0.024
	2	0.136	0.137	0.135	0.135
	3	0.149	0.149	0.147	0.147
	4	0.530	0.525	0.524	0.519
	5	0.566	0.561	0.558	0.554
	6	1.303	1.299	1.274	1.269
0.4	1	0.019	0.018	0.018	0.018
	2	0.113	0.113	0.111	0.110
	3	0.117	0.119	0.116	0.118
	4	0.397	0.386	0.391	0.383
	5	0.425	0.420	0.417	0.411
	6	1.013	1.010	0.989	0.985

with respect to x_3-axis are decoupled so that Tables 3 and 4 separately show frequencies corresponding to the in-plane and out-of-plane vibration modes. Also in Tables 1–4, F.E. solutions by present study are compared with those by ABAQUS's shell elements for the clamped–clamped and clamped–free end

Table 3
Natural frequencies for clamped–clamped arch with monosymmetric section x_3-axis (rad/s)

Shape			Parabolic		Elliptic	
h/l	Mode		Present study	ABAQUS	Present study	ABAQUS
0.2	In-plane	1	1.914	1.910	1.901	1.896
		2	3.802	3.781	3.687	3.667
	Out-of-plane	1	0.450	0.450	0.447	0.447
		2	1.397	1.384	1.387	1.374
		3	2.745	2.721	2.767	2.741
		4	4.062	4.045	4.150	4.128
0.3	In-plane	1	1.481	1.483	1.464	1.464
		2	3.178	3.168	3.115	3.104
	Out-of-plane	1	0.335	0.335	0.330	0.331
		2	1.044	1.033	1.031	1.020
		3	2.244	2.217	2.246	2.216
		4	3.477	3.452	3.558	3.528
0.4	In-plane	1	1.129	1.137	1.112	1.119
		2	2.551	2.549	2.518	2.517
	Out-of-plane	1	0.254	0.255	0.250	0.251
		2	0.775	0.768	0.763	0.756
		3	1.736	1.717	1.726	1.705
		4	2.787	2.765	2.839	2.813

Table 4
Natural frequencies for clamped–free arch with monosymmetric section x_3-axis (rad/s)

Shape			Parabolic		Elliptic	
h/l	Mode		Present study	ABAQUS	Present study	ABAQUS
0.2	In-plane	1	0.125	0.125	0.124	0.125
		2	0.605	0.604	0.605	0.604
	Out-of-plane	1	0.036	0.036	0.036	0.036
		2	0.271	0.269	0.266	0.264
		3	1.083	1.070	1.055	1.042
		4	2.513	2.483	2.478	2.447
0.3	In-plane	1	0.109	0.110	0.108	0.109
		2	0.439	0.436	0.438	0.435
	Out-of-plane	1	0.025	0.025	0.025	0.024
		2	0.192	0.191	0.187	0.186
		3	0.774	0.763	0.751	0.741
		4	1.520	1.521	1.503	1.503
0.4	In-plane	1	0.093	0.095	0.093	0.095
		2	0.326	0.318	0.324	0.317
	Out-of-plane	1	0.019	0.019	0.019	0.018
		2	0.145	0.144	0.140	0.139
		3	0.571	0.563	0.552	0.545
		4	1.517	1.494	1.480	1.456

condition, respectively. In the whole range of arch rise to span ratio, it is shown that the present solutions are in excellent agreement with results by shell elements.

Figs. 8–11 show the normalized frequency variation against the arch rise to span length ratio for monosymmetric arches. In these figures, normalized frequencies are given for the ω/ω_0 where ω_0 is the natural frequency in the limiting case of a straight beam with the same length.

From the results we can find that the normalized frequencies give little difference between parabolic and elliptic arches but the variation tendency and orders of normalized frequencies show different characteristics for two type of boundary conditions. For instance, for the clamped–free boundary condition, all normalized frequencies corresponding to coupled and decoupled vibrational modes decrease as the arch rise to span length ratio becomes large (see Figs. 8 and 10). On the other hand, for the clamped–clamped condition, the third coupled and the first in-plane frequencies increase sharply in low h/l and then decrease as the h/l becomes large (see Figs. 9 and 11). Also as the h/l increases, the second coupled and the first in-plane frequencies decrease more slowly than the first and the third frequencies in the coupled modes and the out-of-plane modes in case of the clamped–free arch (see Figs. 8 and 10).

4.3. Spatial buckling analysis of cantilever curved beams

Fig. 12 shows a thin-walled cantilever curved beam under a horizontal load P whose cross-section is the same as the previous example. F.E. solutions using the nine noded shell element of ABAQUS are presented for comparison. The curved beam in Fig. 12 is modeled using 20 curved beam elements, and 160 and 200 shell elements for curved beams monosymmetric with respect to x_2- and x_3-axis, respectively. Similarly to vibrational modes of monosymmetric arches, buckling modes of arches having cross-sections monosymmetric with respect to x_2-axis are spatially coupled but those of arches monosymmetric with respect to x_3-axis are decoupled so that in-plane and out-of-plane modes are separated.

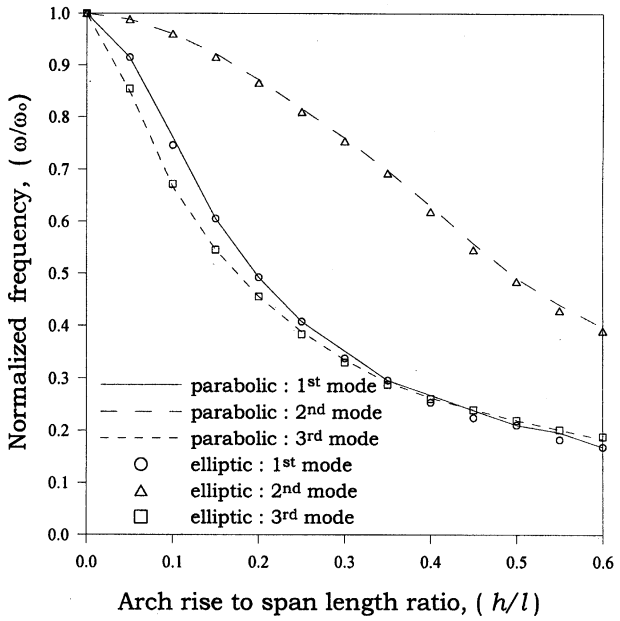

Fig. 8. Effect of rise to span length ratio for clamped–free arch with monosymmetric section x_2-axis.

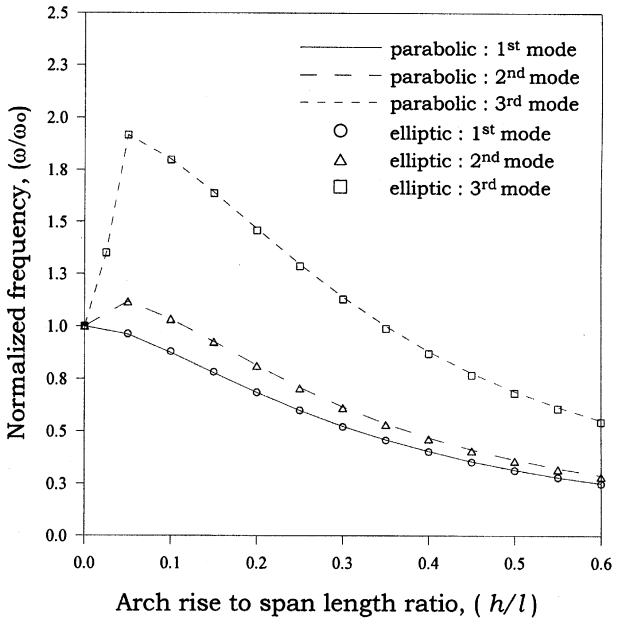

Fig. 9. Effect of rise to span length ratio for clamped–clamped arch with monosymmetric section x_2-axis.

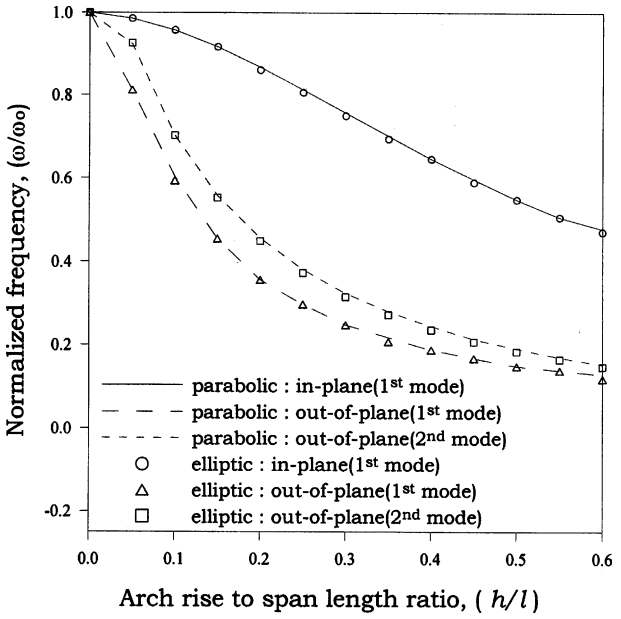

Fig. 10. Effect of rise to span length ratio for clamped–free arch with monosymmetric section x_3-axis.

Lateral–torsional buckling analysis is performed for the loading conditions applied at the free end of the cantilever curved beam. To show effects of the second-order terms of semitangential rotations on buckling load, we consider two cases where CASE1 and CASE2 mean the results by the potential energy Π_G in-

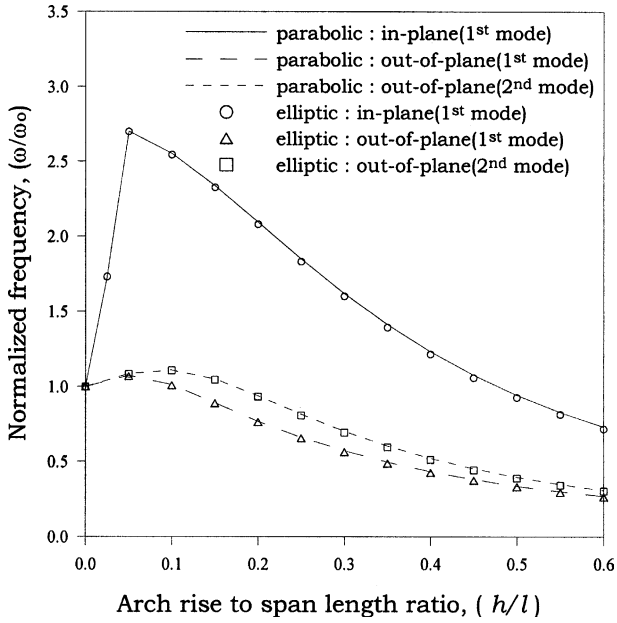

Fig. 11. Effect of rise to span length ratio for clamped–clamped arch with monosymmetric section x_3-axis.

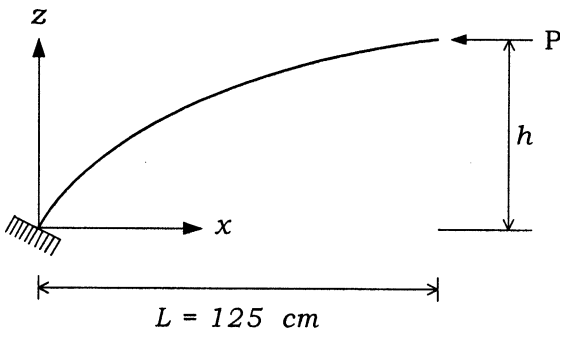

Fig. 12. A cantilever arch and the loading condition for buckling analysis.

cluding the second-order term and by the potential energy Π_{G1} considering only the first-order term, respectively. Tables 5 and 6 show fundamental buckling loads based on CASE1 and CASE2. From Tables, it can be seen that buckling loads by CASE1 coincide closely with the solutions by ABAQUS but CASE2 gives the erroneous results.

In addition, Fig. 13 shows the normalized fundamental lateral–torsional buckling loads against the arch rise to span length ratio for monosymmetric arches. Here normalized buckling load is given for the F/F_0 where F_0 is the lateral–torsional buckling load in a straight beam with the same length. From Fig. 13, it can be found that the normalized lateral–torsional buckling loads give little difference between parabolic and elliptic arches and buckling loads corresponding to coupled and decoupled modes decrease as the arch rise to span length ratio becomes large.

Table 5
Lateral buckling loads for the cantilever curved beam with monosymmetric section x_2-axis

Shape	Parabolic			Elliptic		
h/l	Present study		ABAQUS	Present study		ABAQUS
	CASE1	CASE2		CASE1	CASE2	
0.2	2.774	3.334	2.712	2.676	3.180	2.607
0.3	1.710	2.043	1.652	1.640	1.939	1.581
0.4	1.190	1.411	1.142	1.140	1.338	1.092

Table 6
Lateral buckling loads for the cantilever curved beam with monosymmetric section x_3-axis

Shape	Parabolic			Elliptic		
h/l	Present study		ABAQUS	Present study		ABAQUS
	CASE1	CASE2		CASE1	CASE2	
0.2	4.480	5.621	4.396	4.268	5.281	4.206
0.3	2.602	3.211	2.533	2.466	3.004	2.413
0.4	1.755	2.134	1.701	1.662	1.997	1.619

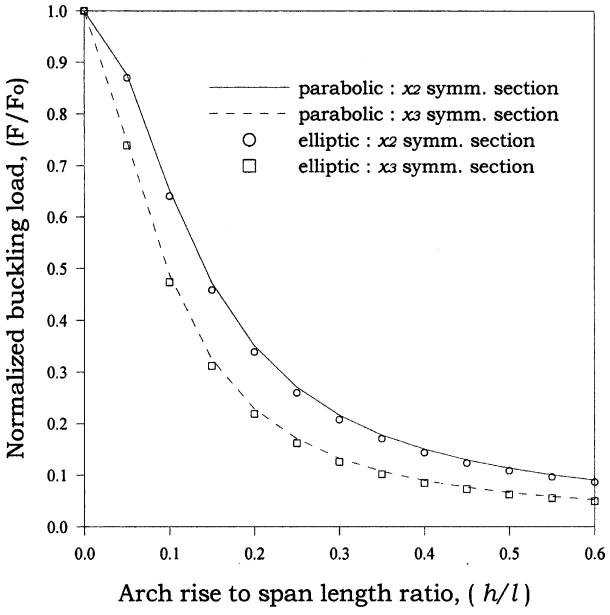

Fig. 13. Normalized lateral–torsional buckling loads for the cantilever curved beam with monosymmetric sections x_2- and x_3-axes, respectively.

5. Concluding remarks

For spatial free vibration and stability analysis of non-symmetric thin-walled curved beams with variable curvatures, the total potential energy of curved beams vibrating harmonically was consistently derived by including the second-order terms of semitangential rotations based on Vlasov's assumption and applying

the principle of linearized virtual work. All displacement parameters of deformation are defined at the centroid axis. The curved beam element having eight degrees of freedom per node was developed in order to investigate the spatial vibrational and buckling behaviour of thin-walled curved beams subjected to general loading and boundary conditions. Through numerical examples, it was shown that the present numerical solutions are in excellent agreement with results by the nine noded shell elements of ABAQUS in the whole range of parabolic and elliptic arch rise to span length ratio. In addition, not only the influences of the arch rise to span length ratio were investigated on spatial vibrational and buckling behaviors of curved beams with the parabolic and elliptic shapes but also it was demonstrated that neglect of second-order term of spatial rotations on lateral–torsional buckling of curved beams may lead to erroneous results.

Acknowledgement

The authors are grateful for the support provided by a grant (R01-2002-000-00265-0) from the Korea Science and Engineering Foundation (KOSEF).

References

ABAQUS, 1992. User's Manual, vols. I and II, Ver. 5.2. Hibbit, Karlsson & Sorensen, Inc.

Argyris, J.H., Symeonidis, Sp., 1981. Nonlinear finite element analysis of elastic systems under nonconservative loading-natural formulation: Part I. Quasistatic problems. Computer Methods in Applied Mechanics and Engineering 26, 75–123.

Argyris, J.H., Hilpert, O., Malejannakis, G.A., Scharpf, D.W., 1979. On the geometrical stiffness of a beam in space—a consistent v.w. approach. Computer Methods in Applied Mechanics and Engineering 20, 105–131.

Chang, S.P., Kim, M.Y., Kim, S.B., 1996. Stability of shear deformable thin-walled space frames and circular arches. Journal of Engineering Mechanics (ASCE) 122 (9), 844–854.

Gutierrez, R.H., Laura, P.A., Rossi, R.E., Bertero, R., Villaggi, A., 1989. In-plane vibrations of non-circular arcs of non-uniform cross-section. Journal of Sound and Vibration 129 (2), 181–200.

Huang, C.S., Tseng, Y.P., Chang, S.H., 1998a. Out-of-plane dynamic response of non-circular curved beams by numerical Laplace transform. Journal of Sound and Vibration 215 (3), 407–424.

Huang, C.S., Tseng, Y.P., Leissa, A.W., Nieh, K.Y., 1998b. An exact solution for in-plane vibrations of an arch having variable curvature and cross section. International Journal of Mechanical Sciences 40 (11), 1159–1173.

Huang, C.S., Tseng, Y.P., Chang, S.H., Hung, C.L., 2000. Out-of-plane dynamic analysis of beams with arbitrarily varying curvature and cross-section by dynamic stiffness matrix method. International Journal of Solids and Structures 37, 495–513.

Kang, Y.J., Yoo, C.H., 1994a. Thin-walled curved beams. I: Formulation of nonlinear equations. Journal of Engineering Mechanics (ASCE) 120 (10), 2072–2101.

Kang, Y.J., Yoo, C.H., 1994b. Thin-walled curved beams. II: Analytical solution for buckling of arches. Journal of Engineering Mechanics (ASCE) 120 (10), 2102–2125.

Kim, M.Y., Min, B.C., Suh, M.W., 2000a. Spatial stability of nonsymmetric thin-walled curved beams. I: Analytic approach. Journal of Engineering Mechanics (ASCE) 126 (5), 497–505.

Kim, M.Y., Min, B.C., Suh, M.W., 2000b. Spatial stability of nonsymmetric thin-walled curved beams. II: Numerical approach. Journal of Engineering Mechanics (ASCE) 126 (5), 506–514.

Kim, S.B., Kim, M.Y., 2000. Improved formulation for spatial stability and free vibration of thin-walled tapered beam and space frames. Engineering Structures 22 (5), 446–458.

Kim, M.Y., Chang, S.P., Park, H.G., 2001. Spatial postbuckling analysis of nonsymmetric thin-walled frames. I: Theoretical considerations based on semitangential property. Journal of Engineering Mechanics (ASCE) 127 (8), 769–778.

Kuo, S.R., Yang, Y.B., 1991. New theory on buckling of curved beams. Journal of Engineering Mechanics (ASCE) 117 (8), 1698–1717.

Love, A.E.H., 1934. A treatise on the mathematical theory of elasticity, fourth ed. University press, Cambridge.

Oh, S.J., Lee, B.K., Lee, I.W., 2000. Free vibration of non-circular arches with non-uniform cross-section. International Journal of Solids and Structures 37, 4871–4891.

Oh, S.J., Lee, B.K., Lee, I.W., 1999. Natural frequencies of non-circular arches with rotatory inertia and shear deformation. Journal of Sound and Vibration 219 (1), 23–33.

Papangelis, T.P., Trahair, N.S., 1987a. Flexural–torsional buckling of arches. Journal of Structural Engineering (ASCE) 113 (4), 889–906.

Papangelis, T.P., Trahair, N.S., 1987b. Flexural–torsional buckling test on arches. Journal of Structural Engineering (ASCE) 113 (7), 1433–1443.

Romanelli, E., Laura, P.A.A., 1972. Fundamental frequencies of non-circular, elastic, hinged arcs. Journal of Sound and Vibration 24 (1), 17–22.

Saleeb, A.F., Chang, T.Y.P., Gendy, A.S., 1992. Effective modelling of spatial buckling of beam assemblages accounting for warping constants and rotation-dependency of moments. International Journal for Numerical Methods in Engineering 33, 469–502.

Tarnopolskaya, T., de Hoog, F., Fletcher, N.H., Thwaites, S., 1996. Asymptotic analysis of the free in-plane vibrations of beams with arbitrarily varying curvature and cross-section. Journal of Sound and Vibration 196 (5), 659–680.

Timoshenko, S.P., Gere, J.M., 1961. Theory of elastic stability, second ed. McGraw-Hill, New York.

Tseng, Y.P., Huang, C.S., Kao, M.S., 2000. In-plane vibration of laminated curved beams with variable curvature by dynamic stiffness analysis. Composite Structures 50, 103–114.

Tseng, Y.P., Huang, C.S., Lin, C.J., 1997. Dynamic stiffness analysis for in-plane vibrations of arches with variable curvature. Journal of Sound and Vibration 207 (1), 15–31.

Usuki, S., Kano, T., Watanabe, N., 1979. Analysis of thin walled curved members in account for large torsion. Proceedings of JSCE (290), 1–15.

Vlasov, V.Z., 1961. Thin-walled elastic beams, second ed. National Science Foundation, Washington, DC.

Wang, T.M., 1972. Lowest natural frequency of clamped parabolic arcs. Journal of Structural Division 98 (ST1), 407–411.

Wang, T.M., Moore, J.A., 1973. Lowest natural extensional frequency of clamped elliptic arcs. Journal of Sound and Vibration 30 (1), 1–7.

Yang, Y.B., Kuo, S.R., 1987. Effect of curvature on stability of curved beams. Journal of Structural Engineering (ASCE) 113 (6), 1185–1202.